Polymer Degradation and Stability 109 (2014) 293–306

Contents lists available at ScienceDirect

Polymer Degradation and Stability

journal homepage: www.elsevier.com/locate/polydegstab

Structure, physical properties, biocompatibility and *in vitro*/*vivo* degradation behavior of anti-infective polycaprolactone-based electrospun membranes for guided tissue/bone regeneration

Rui Shi [a], Jiajia Xue [b], Min He [b], Dafu Chen [a], Liqun Zhang [b, *], Wei Tian [a, c, **]

[a] Laboratory of Bone Tissue Engineering of Beijing Research Institute of Traumatology and Orthopaedics, Beijing 100035, China
[b] Beijing Laboratory of Biomedical Materials, Beijing University of Chemical Technology, Beijing 100029, China
[c] Department of Spine Surgery of Beijing JiShuiTan Hospital, The Fourth Clinical Medical College of Peking University, Beijing 100035, China

ARTICLE INFO

Article history:
Received 19 May 2014
Received in revised form
14 July 2014
Accepted 18 July 2014
Available online 28 July 2014

Keywords:
Polycaprolactone
Metronidazole
Gelatin
Electrospinning
Guided tissue regeneration

ABSTRACT

Nanofiber membranes composed of polycaprolactone (PCL), PCL/metronidazole (MNA), PCL/gelatin/MNA, and PCL/gelatin/MNA/acetic acid (HAC), named P0, P30, PG30, and PGH30, respectively, were fabricated by electrospinning for application in guided tissue/bone regeneration (GTR/GBR) therapies. The architectural features, mechanical properties, hydrophilicity, drug-encapsulation efficiency, drug-release pattern, antimicrobial properties, cell barrier functions, *in vitro*/*vivo* degradability and biocompatibility were investigated. All membranes were found to have high tensile strength, which is required for GTR applications. Strong interactions among PCL, gelatin, and MNA resulted in high drug loading efficiency, which was further improved by the incorporation of gelatin and HAC. MNA incorporation gave the membranes good antimicrobial property, while reducing host versus graft reaction, improving the hydrophilicity and accelerating the degradation. Gelatin incorporation considerably improved cytocompatibility, while accelerating the degradation dramatically. Very low quantities (0.1% v/v with respect to polymer solution) of HAC effectively prevented the phase separation of PCL and gelatin, resulting in homogeneous nanofiber, which facilitates stable physical properties. The drug-release profiles of all drug-loading membranes were consistent with the inflammation cycle characteristics. High drug loading and trace amounts of HAC did not cause any adverse reactions, as evidenced by subcutaneous implantation. Both P0 and P30 maintained their cell barrier function *in vivo* for as long as 24 weeks; PGH30, for 8 weeks; and PG30, for less than 8 weeks. These findings enabled a comprehensive understanding of the influence of different compositions on the structure and performance of the membranes, thereby supporting the design of membranes with superior overall performance for GTR/GBR application.

1. Introduction

Guided tissue/bone regeneration (GTR/GBR) techniques have been successfully applied for treating periodontal lesions and have provided the opportunity to form new bone [1]. This technique utilizes membranes as mechanical barriers to create a space around the defects, permitting bone regeneration to occur in the absence of competition for space by the surrounding connective tissues. Membranes used in GTR/GBR therapy must be biocompatible, have the proper degradation profile and adequate mechanical and physical properties, and sufficient sustained strength [2].

Electrospun nanofibrous scaffolds/membranes more closely mimic the scales and morphologies of extracellular matrix (ECM) proteins (fiber diameters range from 50 to 500 nm). The inherently high surface to volume ratio of electrospun scaffolds can enhance cell attachment, drug loading, and sustained and controlled local drug delivery [3,4]. The average pore size of the electrospun nanofiber membrane is approximately 4–6 μm. Eukaryotic cell diameters range from 10 to 100 μm. It is difficult for gingival fibroblasts and periodontal cells to pass through an electrospinning membrane. These structural characteristics make the electrospun nanofibrous membranes very suitable for use as a GTR/GBR membrane.

* Corresponding author. Tel.: +86 010 64421186; fax: +86 010 64433964.
** Corresponding author. Department of Spine Surgery of Beijing JiShuiTan Hospital, The Fourth Clinical Medical College of Peking University, Beijing 100035, China. Tel./fax: +86 010 58516718.
E-mail addresses: zhanglq@mail.buct.edu.cn (L. Zhang), tianweia@163bj.com (W. Tian).

http://dx.doi.org/10.1016/j.polymdegradstab.2014.07.017
0141-3910/

GTR membranes can be non-biodegradable or biodegradable. Non-biodegradable membranes require a second surgical procedure for membrane removal. Biodegradable membranes allowing a single-step procedure reduce patient discomfort. Collagen is the most widely used natural biomaterial for GTR application. However, there are some limitations, such as the loss of space maintenance under physiological conditions, risks of disease transmission to humans from animal-derived collagen, and high cost [5]. To overcome these limitations, polymeric GTR membranes were developed. Poly (lactic acid) (PLA), poly(glycolic acid) (PGA), and their copolymers have been widely considered for GTR membrane applications. However, the accumulation of acid during degradation may significantly reduce pH, resulting in chronic aseptic inflammation [6].

Compared to PLA and PGA, PCL degradation does not produce a local acidic environment. Thus, because of its comparatively low cost and high mechanical strength, PCL is an attractive biomedical polymer. However, only a few studies have examined PCL-based GTR membranes [7,8]. PCL degrades very slowly. The absorption time of PCL *in vivo* is approximately 2–3 y [5,9], which is too long for application in GTR/GBR treatment. Furthermore, its poor hydrophilicity reduces cell adhesion. Therefore, PCL is blended or copolymerized with other polymers before biomedical application.

Among electrospun biodegradable polymers, electrospinning of hybrids, particularly natural and synthetic polymer blends, has received increasing attention [10,11]. Gelatin, the hydrolysis product of collagen, can be completely absorbed quickly. It is also biocompatible, biodegradable, and a major component of the native ECM. Gelatin is non-immunogenic and retains informational signals such as the arginine–glycine–aspartic acid sequence, which promotes cell adhesion, differentiation, and proliferation [12]. Thus, gelatin was combined with PCL to form a composite GTR membrane.

However, poorly blended polymeric fibers are generated with porous or phase-segregated internal structures as a result of the weak molecular interactions between natural and polymeric polymers. This is particularly true when the natural biopolymer component reaches a threshold percent. Intense phase separation was observed in electrospun collagen/PCL hybrids when the PCL component was increased to 30% [13], and severe phase segregation occurred when the components were blended in equal parts for the cases of electrospun gelatin/PCL [14] and electrospun collagen/PLCL [15]. Therefore, controlling the formation of homogeneous internal structures of electrospun nanofibers by modulating the miscibility of solutions containing both natural and synthetic components is critical. Incorporating a tiny amount of acetic acid may allow the originally turbid solution to become immediately clear and to be single-phase stable for more than 1 week [16]. Some structural and physical properties of the PCL/gelatin/HAC composites have been studied. However, biosecurity, degradation, and foreign body reaction following incorporation of acetic acid have not been reported. In addition, PCL/gelatin/HAC composites used to prepare the drug loading GTR/GBR membrane have not been determined.

The presence of periodontopathogens such as *Porphyromonas gingivalis* and *Prevotella intermedia* may negatively affect the success of periodontal regeneration. Therefore, it is very important to control and/or reduce bacterial contamination of the periodontal defect to enhance periodontal regeneration [17]. Metronidazole (MNA) has been used to treat infections for more than 45 y and is still successfully used for treating anaerobic bacterial infections. Although systemic administration of antibiotics is useful, high oral doses are necessary to achieve effective concentrations in the gingival fluid. However, long-term use may lead to the development of resistant bacterial strains. These limitations have led researchers to examine localized delivery of antibiotics directly at the diseased site [18]. Electrospun nanofiber membranes are used to achieve different controlled drug release profiles in drug delivery applications [19]. MNA has been integrated into PLA and PLGA nanofibers for local periodontitis treatment. This drug delivery system showed sustained drug release and significantly decreased bacterial viability [20]. In addition, significant improvement in periodontal regeneration following GTR was observed in dogs [21]. Although a derivative of MNA has been mixed with PCL to fabricate nanofibrous scaffolds, but PCL-based matrix loading of MNA for GTR/GBR application has not been reported. The effects of the interaction between the drug and polymer matrix on the physical–chemical properties, drug release profile, and long-term *in vivo* biocompatibility and biodegradability of the drug delivery system have not been thoroughly investigated.

In this study, electrospinning technology was used to fabricate 4 types of PCL-based GTR membranes composed of PCL, PCL/MNA, PCL/gelatin/MNA, and PCL/gelatin/MNA/HAC. The effects of the material components on the physical and chemical structure, mechanical and thermal properties, barrier function, antimicrobials performance, histocompatibility, and *in vitro* and *in vivo* degradation of different membranes were investigated in detail. The results of this study would render technology and material references for preparation of GTR/GBR membranes with excellent comprehensive properties.

2. Materials and methods

2.1. Preparation of electrospun PCL-based nanofiber membranes

The materials used in this study are listed in Electronic Supplementary Information (ESI) S1. Composition and preparation of the spinning solution are stated in ESI S2. Membranes with different compositions were fabricated according to the conventional electrospinning procedure are also described in S2.

2.2. Characterization of PCl-based nanofiber membranes

2.2.1. Morphology

Membrane morphology was observed using a scanning electron microscope (SEM) (S4700, Hitachi Co., Tokyo, Japan) at a voltage of 20 kV. The membranes were coated with gold and observed under the microscope. Fiber diameter and pore size were measured using the ImageJ software from SEM micrographs at random locations ($n = 100$). Membrane thickness was measured using a micrometer, and its apparent density and porosity was estimated using equations eq.s1 and eq.s2 (see ESI S3) [22].

2.2.2. Molecular dynamic simulation

Molecular dynamics simulation was used to investigate the effect of drug content in the polymer. The Discover and Amorphous Cell modules of the Materials Studio suite were used (Accelrys, San Diego, CA, USA) [23]. All theoretical calculations were performed using the condensed-phase optimized molecular potentials for atomistic simulation studies (COMPASS) force field (see ESI S4).

2.2.3. Thermal, crystal, and chemical structure and mechanical property

Fourier transform infrared spectroscopy (FTIR), differential scanning calorimetry (DSC), and X-ray diffraction (XRD) analyses (see ESI 5) were performed to investigate the chemical and thermal properties of the membranes. Tensile strength (TS) and elongation at break (EB) of the membranes both in the dry and wet states were evaluated using a BOSE ElectroForce 3200 test instrument (Framingham, MA, USA) (see ESI S5).

2.2.4. Surface hydrophilicity

Membrane hydrophobicity was determined by measuring the static water contact angle (CA). Water CAs were measured using a SL200A type Contact Angle Analyzer (Solon (Shanghai) Technology Science Co., Ltd., Shanghai, China).

2.2.5. Drug entrapment efficiency and drug release profile

Entrapment efficiency was determined by dissolving a known mass of membrane in 1 mL of dimethylformamide and then added to 20 mL methanol drop by drop. After centrifugation, the liquid supernatant was analyzed by high-performance liquid chromatography (HPLC) at $\lambda_{max} = 310$ nm. The amount of MNA was determined from the calibration curve of MNA. Entrapment efficiency was calculated as:

$$\text{Encapsulation efficiency } \% = \frac{\text{weight of drug in the sample(g)}}{\text{theoretical weight of drug loading in the sample(g)}} \times 100\%$$

The drug release profile of the membranes was detected by soaking the membrane in phosphate-buffered saline (PBS). The membrane was cut into a circle of 2-cm diameter, accurately weighed, and then rinsed in 5 mL PBS solution (pH 7.4) in a container. The containers were sealed and placed in a water bath shaker at 100 rpm and 37 °C. At predetermined time intervals, 2 mL PBS was removed for HPLC detection and another 2 mL fresh PBS was added. The amount of drug released was determined by HPLC.

2.2.6. In vitro biodegradation

The membrane was cut into a circle of 2-cm diameter (an average of three for each membrane), weighed, and soaked in 12-well plates with 5 mL PBS at 37 °C. At predetermined time intervals, the remaining sample was carefully removed from the well, rinsed thrice using MilliQ water, dried at 50 °C until the mass remained unchanged, and then weighed. The mass remaining vs. time was plotted to obtain the degradation profile of the membrane. The morphology of the nanofiber during degradation was observed by SEM.

2.3. In vitro biocompatibility, barrier function, and antibacterial activity evaluation

2.3.1. Biocompatibility

The cytotoxicity of the membranes to L929 fibroblast cells, human periodontal ligament fibroblasts (hPDLFs), and Rat Osteoblast-like (ROS) cells was evaluated (see ESI 6). A Cell Counting Kit-8 (CCK-8) assay was performed to test the attachment and proliferation of L929 fibroblast cells on membranes (see ESI S7).

2.3.2. Barrier function to fibroblast cells

The *in vitro* barrier function of the membrane in L929 cells being used as model cells was tested as follows (Fig. 1): The membrane was cut into a circle 2.5 cm in diameter, sterilized, fixed on a Cell-Crown, and then placed into 24-well plate without touching the bottom of the well. L929 cells were resuspended in Dulbecco's Modified Eagle Medium supplemented with 10% (v/v) fetal bovine serum at a density of 4.0×10^4 cells/mL. Next, 1 mL culture medium without cells was added to the well from the outside of the Cell-Crown, and 900 μL culture medium plus 100 μL cell resuspension was added to the sample. After incubation at 37° under a 5% CO_2 atmosphere for 1, 3, 5, and 7 days, the Cell-Crown was removed and the bottom of the 24-well plate was observed under an inverted phase contrast microscope (IX50-S8F2, Olympus, Tokyo, Japan) to investigate whether the cells had passed through the membrane to the bottom of the well or the culture medium. The other side of the membrane, which had no contact with the cells, was observed by SEM to determine whether the cells had penetrated the membrane. The barrier function of the membrane after 1 month of degradation in PBS was also tested as described above.

2.3.3. Antibacterial activity

Antibacterial activity of the membranes against anaerobic bacteria *Fusobacterium nucleatum* (ATCC 25586, Chinese General Microbiological Culture Collection Center), which is commonly found in the oral cavity during infection, was determined using the modified Kirby–Bauer method (see ESI S8) as previously described [24].

2.4. In vivo biocompatibility and biodegradability

Thirty healthy adult male New Zealand white rabbits (2.5–3 kg each) were used as experimental animals. The protocol was approved by the Animal Ethical Committee of Beijing Jishuitan Hospital, and national guidelines for the care and use of laboratory animals were applied. Prior to initiating the animal experiment, the membranes (1.5×1.5 cm^2) were sterilized by γ-irradiation (Isotron, Ede, Nederlands). The animals were anesthetized with isoflurane,

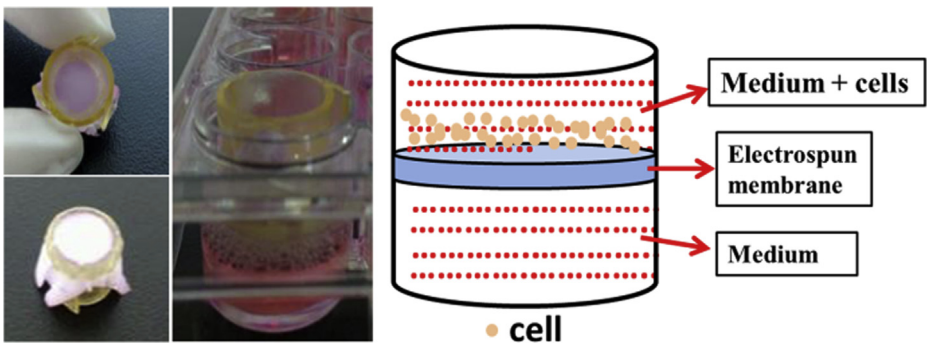

Fig. 1. The photographs and schematic diagram of barrier function characterization of electrospun nanofiber membrane.

and their backs were shaved and sterilized with alcohol and iodine scrub. Six par vertebral incisions (2 cm each) per rabbit were made approximately 1 cm lateral to the vertebral column to expose the dorsal subcutis. Subcutaneous pockets were created by blunt dissection. Each individual pocket held one membrane, and the incisions were closed using surgical sutures. All the surgeries were carried out in an aseptic field using aseptic technique. After being implanted for 1, 3, 5, 8, 12, and 24 weeks, membranes were taken out and observed histologically and by SEM (see ESI S9).

2.5. Statistical analysis

The data obtained from each membrane for results from mechanical test, mass loss value, and drug loading efficiency were averaged and expressed as the mean ± standard deviation. Significant differences among different membranes with the same composition were determined using the *t*-test. Differences were considered statistically significant at a p value of <0.05.

3. Results

3.1. Surface morphology

PCL-based nanofiber membranes approximately 250-μm thick were obtained through 20 h of electrospinning. The surface morphology of membranes P0, P30, PG30, and PGH30, as well as their fiber diameter distribution are shown in Fig. 2. Electric conductivity (EC) of different electrospinning liquid, pore size, and porosity values of different membranes are listed in Table 1.

Micrograph images of the pure PCL nanofiber showed a randomly interconnected structure, smooth morphology, and uniform distribution of the electrospun nanofiber with no beads formed. Following addition of MNA (P30), the electrical conductivity of the spinning solution increased, while the fiber's diameter, pore size and porosity of the membrane decreased (Table 1). For PG30, the spinning liquid was transparent when PCL/HFIP and gelatin/HFIP solutions were mixed together and electrical conductivity of the mixed solution dramatically increased. However, after 3–4 h, the mixed solution became opaque and gradually separated into different phases upon standing and formed clear sediment by 8–12 h. The phase boundary of the solution is indicated in Fig. S2 (see ESI S10) PG30 as a red arrow. During gelatin incorporation, fiber diameter distribution became non-uniform. Based on the fiber diameter, the fibers can be divided into thick (1.51 ± 0.3 μm diameter) and thin (0.30 ± 0.1 μm diameter) groups. Phase separation led to non-uniform fiber morphology.

For PGH30, a very small amount of HAC (0.1% of the total spinning liquid volume) was added to the spinning solution. The mixture immediately changed from turbid to clear, even after 24-h incubation under ambient conditions (see Fig. S2 in ESI S10). The resulting fibers were smooth and uniform, with an average fiber diameter of 0.97 ± 0.20 μm (Table 1).

The mean pore size of nanofiber membranes ranged from 3 to 6 μm. The pore size of P0 was 6.04 ± 0.64 μm, with a porosity of 76.4%. When mixed with other components, pore sizes decreased to 3–4 μm, while porosity decreased to approximately 70%. Several small particles on surface of the drug loading membranes were observed. The number of crystal particles on PGH30 appeared to be lower than that on PG30.

3.2. Molecular dynamics simulation of hydrogen bonds (HBs) between PCL and MNA

HBs between the MNA and PCL matrix of nanofiber membranes with different MNA content were simulated by molecular dynamics simulation using the Materials (Accelrys, San Diego, CA, USA)Studio software (Accelrys, San Diego, CA, USA). The PCL chains and MNA molecules were built in an amorphous cell to calculate the number, length, and angle of (Accelrys, San Diego, CA, USA)HBs, with the MNA to PCL weight to mass ratio fixed at 1, 5, 20, and 40%. As shown in Fig. S3 in ESI S11, the oxygen and nitrogen atoms of −OH, C═N, and $-NO_2$ on MNA can hydrogen bond with the hydrogen atom of −CH on PCL, and the hydrogen atom of $-NO_2$ and −OH on MNA can form hydrogen bonds with PCL ester groups. Simulation showed that at low drug loading (5%), MNA was homogeneously dispersed in the polymer, but as drug loading increased to over 20%, MNA molecules generally formed hydrogen bond with each other and aggregated.

3.3. Chemical, crystallization, thermal, and mechanical properties

FTIR was used to investigate HB interactions among different components and to determine whether a chemical reaction had occurred. During spinning, DSC and XRD measurements were used to investigate PCL and MNA crystallinity, drug distribution, and acetic acid-mediated homogeneity of the nanofiber membranes (Fig. 3). TS and EB of the membranes both in the dry and wet states were measured (Table 2).

FTIR results showed that the characteristic peaks of MNA on the spectra of P30, PG30, and PGH30 did not differ from those of pure MNA crystals, demonstrating that the electrospinning process did not adversely affect the molecular structure of MNA, particularly the antibacterial $-NO_2$ group. Acetic acid did not react with other components during electrospinning. Shifting of the original absorption bands towards the lower wave numbers indicated that HBs existed among PCL, gelatin, and MNA molecules, which is consistent with the results of molecular dynamics simulation. DSC and XRD results demonstrated that the melting enthalpy (ΔHm) and crystallinity of the PCL matrix decreased (Table.S1 in ESI S12) after MNA incorporation. When gelatin was added, ΔHm and PCL matrix crystallinity further decreased. However, ΔHm and MNA crystallinity increased, while the melting point increased. For PGH30, ΔHm and PCL matrix crystallinity decreased and ΔHm of MNA also decreased unlike that in the case of PG30 (see ESI S12).

TS and EB of the MNA drug loading membrane (P30) was lower than the values for pure PCL (P0). With the incorporation of additional gelatin, mechanical strength further decreased. Though the miscibility between PCL and gelatin in PGH30 was better than that in PG30, the mechanical properties showed no obvious changes. TS of dry and wet PGH30 were similar, while other membranes showed slightly higher TS in the wet state than in the dry state.

3.4. Surface hydrophilicity

We measured the static water CA and observed the shape of a water droplet on the nanofiber membrane surface at 5 s (Fig. S4 in ESI S13). CA values are listed in Table 3. Water CA measurement results confirmed that both MNA and gelatin can significantly improve the hydrophilicity of the nanofiber membrane; the CA value of PGH30 was increased compared to PG30, suggesting a slight decrease in hydrophilicity.

3.5. Drug encapsulation efficiency and drug release profiles

Calculated encapsulation efficiency values for P30, PG30, and PGH30 were 83.2 ± 1.1, 84.9 ± 1.5, and 85.7 ± 0.9, respectively. All the membranes achieved a high drug loading efficiency of above 80%, demonstrating that both the PCL and PCL/gelatin composite nanofibers are good carriers for hydrophilic drugs. Incorporation of

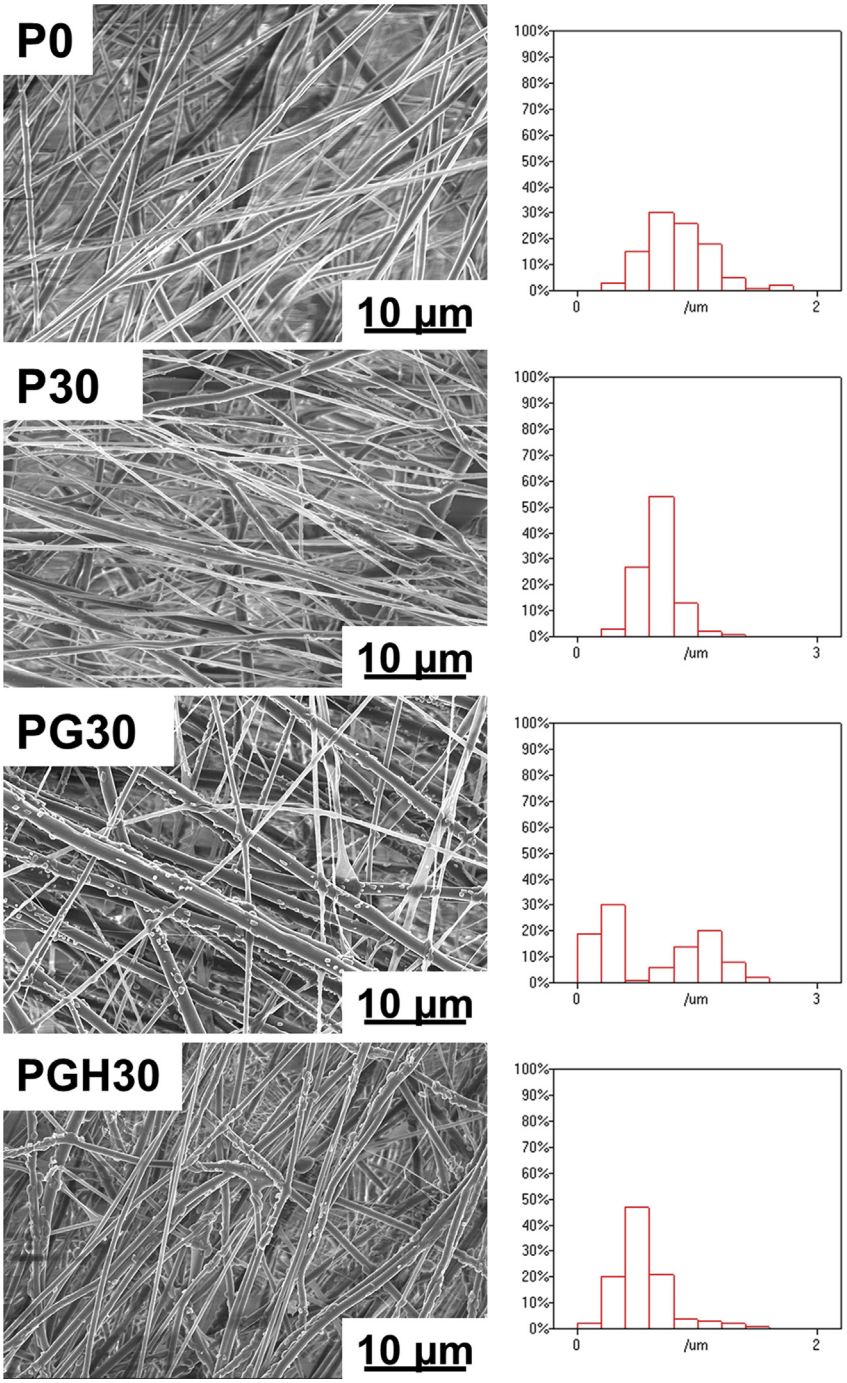

Fig. 2. SEM micrographs of PCL based GTR membranes.

gelatin and trace amounts of acetic acid contributed to drug loading.

Fig. 4 shows the release profiles of different nanofiber membranes with the same amount of MNA. All the samples released above 90% MNA within 1 week and showed a large initial burst release. Subsequently, drug release was linear from 7 to 14 days. The cumulative drug release of all the membranes reached more than 97% in 14 days. After a period of 7 days, the drug release rates slowed until accumulated drug release was nearly steady; thus, almost no variance is observed in the figure. The drug release profiles of P30 and PG30 were similar. However, the drug release rate of PGH30 was slower than those of both P30 and PG30 from days 5–14.

3.6. *In vitro* degradation behavior

In vitro degradability of membranes was also investigated gravimetrically (Fig. 5). Morphological changes in nanofiber membranes after 30 days of degradation were observed by SEM (Fig. S5 in ESI S14). A local enlarged image is placed in the upper right corner of each SEM image. SEM morphology revealed that the overall gross morphology of P0 after degradation for 30 days showed no significant difference. However, for P30, PG30, and PGH30, a small number of microcracks and voids were observed on the nanofiber surface. Surface roughness increased and fiber fractures were present, unlike that in the pre-degradation samples.

Table 1
Electrical conductivity of the spinning solution as well as the pore size and porosity of membranes.

Sample	Pore size (μm)	Porosity (%)	Electrical conductivity (μs/cm)
P0	6.04 ± 0.64	76.4	6.43 ± 1.32
P30	3.04 ± 0.50	70.2	7.41 ± 1.48
PG30	3.21 ± 0.80	70.5	18.63 ± 2.25
PGH30	4.01 ± 0.70	70.9	19.04 ± 1.39

Table 2
TS and EB of the different PCL-based membranes in dry and wet state.

Samples	Dry state		Wet state	
	TS (Mpa)	EB (%)	TS (Mpa)	EB (%)
P0	9.99 ± 1.02	325 ± 35	12.55 ± 2.82	152 ± 16
P30	6.33 ± 0.84	99 ± 27	11.84 ± 1.27	52 ± 16
PG30	4.14 ± 0.90	19 ± 3	6.23 ± 1.53	13 ± 4
PGH30	4.26 ± 1.17	24 ± 6	3.88 ± 0.49	30 ± 9

In the first 3 months, the hydrolysis rate of P0 was very slow; only 10 wt% of the material degraded, with the most mass lost after 2 months (Fig. 5). For the other samples, the mass quickly decreased during the first 2 weeks of degradation. For P30, the calculated drug percentage was 19.2% (calculation method is in ESI S14), which was similar to the value after 2 weeks of degradation. Thus, the mass decrease of P30 was mainly caused by drug release during the first 2 weeks. Because of the high water solubility of gelatin, the PG30 degradation rate was much higher than that of P30. The calculated total weight percentage of the gelatin and MNA was 59.1% (see ESI S14). Additionally, the mass decreased by 52% after 3 months of degradation, which is similar to the total mass percentage of MNA and gelatin. The mass loss of PGH30 after 3 months was 59.6%, which is also similar to the total mass percentage of MNA and gelatin. These results demonstrate that drug release and gelatin dissolution were the main factors affecting degradation in the first 3 months *in vitro*.

The mechanical properties of the nanofiber membranes after degradation for 30 days were also tested to determine whether the membrane could prevent fibroblast cell infiltration into the tissue defect site and support new tissue growth. The results are shown in Table S2 (see ESI S15). TS only showed a slight decrease after 1 month of degradation, which was maintained at approximately 2–6 MPa. This satisfied the requirement for the GTR/GBR membrane [25,26].

3.7. Cell experiments

3.7.1. Cytotoxicity

After 72 h, L929 cells incubated in the extract substrates of different electrospun membranes presented spindle, triangle, and quadrangle shapes (see Fig. S6 in ESI S16), which revealed very good cellular growth. The high MNA concentration (even in the extract substrates of membranes with a high MNA content of 30%) did not affect cell growth. After 72 h of incubation, cells in the PG30 leaching solution showed higher relative growth rates (RGRs) than those in the other samples, and even higher than those in the negative control. The RGR of PGH30 reached 93% (Fig. 6). Trace amounts of acetic acid were not cytotoxic, but the cytotoxicity of PGH30 was grade 1 (see eq. S3 in ESI S16).

Based on these results and because of the prevalence of osteoblasts and hPDLFs around tooth defects, we tested the cytotoxicity of P30 with hPDLFs and ROS cells. The fluorescence intensity of hPDLFs and ROS cells cultured for 24 h in the extract solution are shown in Fig. S7 in ESI S17. Compared with controls, the RGRs of both the cell types were >100%, indicating that the membrane did not adversely affect the viability of hPDLFs and ROS cells.

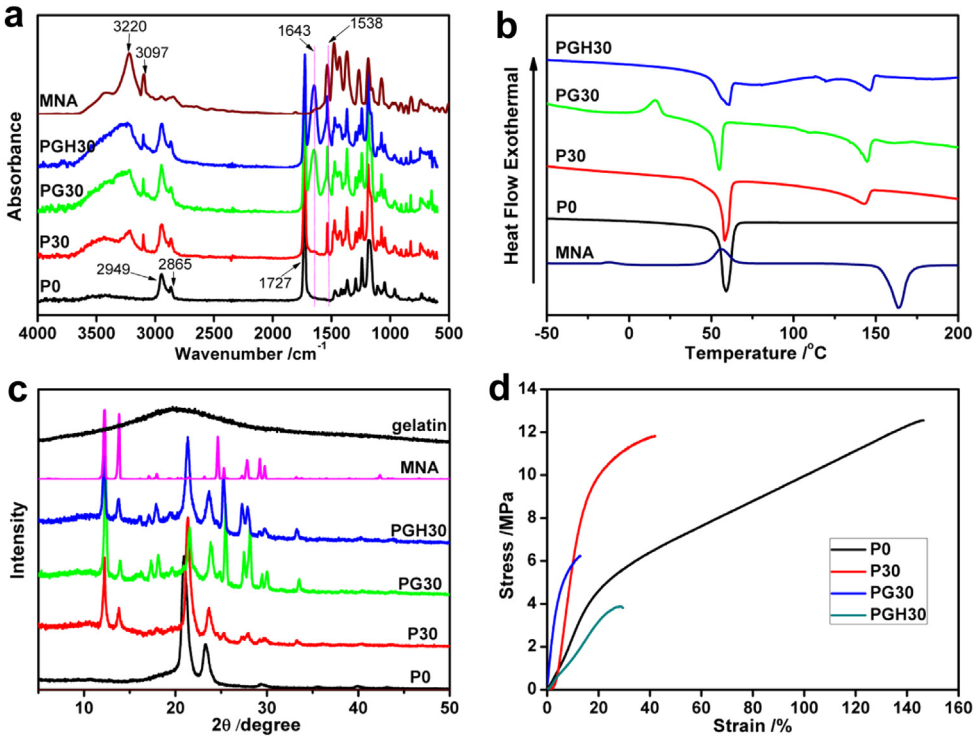

Fig. 3. Chemical, thermal, and mechanical properties of PCL-based nanofiber membranes: (a) FTIR spectra, (b) DSC thermograms, (c) XRD patterns, and (d) stress–strain curves of membranes in wet state.

Table 3
Water contact angle values of electrospun PCL-MNA nanofiber membranes.

Samples	CA (°)
P0	129.64
P30	83.99
PG30	36.69
PGH30	61.16

3.7.2. Attachment and proliferation of L929 fibroblast to membranes

A CCK-8 assay was performed to examine the influence of MNA on the adhesion and proliferation of L929 cells on different electrospun nanofiber membranes. The RGR of the L929 cells adhered on the nano-fibrous membranes and TCP (the control) after being seeded for 4 h are shown in Fig. 7a. L929 cells adhered to all of the PCL-based membrane well. L929 cells attached to P0 and P30 showed no significant difference and were fewer cells than those attached on TCP; however, cells adhered on PG30 and PGH30 are nearly as same as those on TCP. Gelatin addition significantly improved cell attachment. Cells attached on PG30 and PGH30 showed no statistical differences, demonstrating that HAC contained in PGH30 did not adversely affect cell attachment.

RGRs of L929 cells proliferated for 1, 3, 5, and 7 days on the electrospun nanofiber membranes tested at 450 nm using the CCK-8 assay are shown in Fig. 7b. The number of cells increased continuously over 7 days of culture for pure PCL (P0) and the MNA loading membrane (P30). The proliferation rate of L929 on P30 was faster than that on P0. Gelatin greatly increased L929 cell proliferation, as the cell number on the surface was sufficiently high on the first day, and the RGR of L929 cells changed very little over the 7 days for PG30 and PGH30. HAC contained in PGH30 appeared to have little influence on cell vitality from 1 to 7 days when compared with PG30, but the cell number on PGH30 remained sufficiently high to reach an estimated confluency of approximately 90%.

To observe the effects of different components on fibroblasts, SEM studies were carried out on membranes on days 1, 3, 5, and 7. The cellular morphology on different membranes on the 1st and 7th days is shown in Fig. 7c and d. A larger number of interactions and contacts were present among cells on PG30 and PGH30 than on P0 and P30 on the 1st day. On the 7th day, only 50–60% L929 cell confluence was observed, and the cells were primarily round shaped cells on P0 and P30, but reached an estimated confluency of approximately 90% on PG30 and PGH30 (see ESI S18).

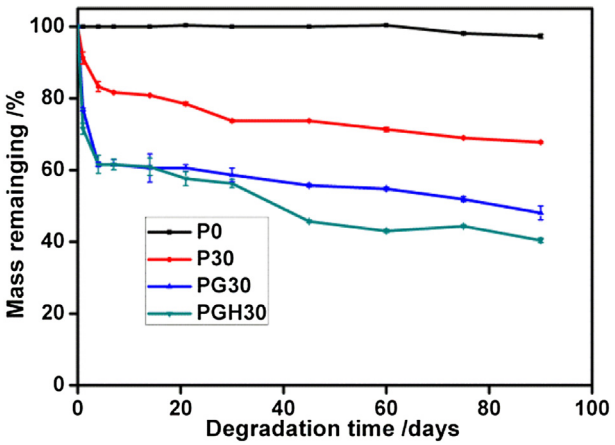

Fig. 5. Mass loss during *in vitro* degradation of electrospun PCL-based nanofiber membranes.

3.8. Barrier function to fibroblast cells

In order to test the cell barrier function of the PCL-based membranes, we designed a novel method *in vitro* (See Fig. 1). SEM Micrographs of the surface of the opposite side which had no contact with the cells after culture for 3 days are shown in Fig. 8. For all the PCL-based membranes, even after seeding cells for 3 days, no L929 cells were observed on surface of this side perfectly illustrates that the membranes had good cell barrier function. The same results were obtained after 1 month of degradation.

3.9. Antibacterial function

The growth of *F. nucleatum* was visualized directly on plates to assess antibacterial activity (Fig. 9a). The inhibition zone diameters of the membranes at different incubation times are displayed in Fig. 9b. Agar plates with P0 membranes were completely covered with bacteria after incubation, but agar plates with drug-loaded membranes showed inhibition of bacterial growth that persisted for the 30 days of the incubation. Inhibition zone diameters of gelatin-containing samples were larger than that for the without gelatin samples over 30 days. The inhibition zone decreased as an additional drug was released; however, even after one month, there

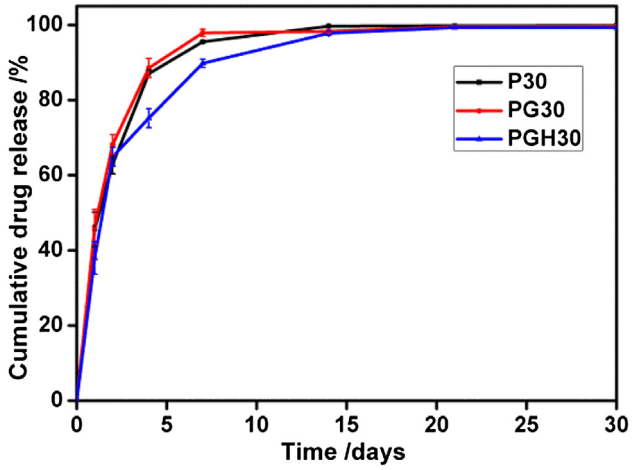

Fig. 4. The cumulative drug release percentage of membranes at different soaking time in PBS.

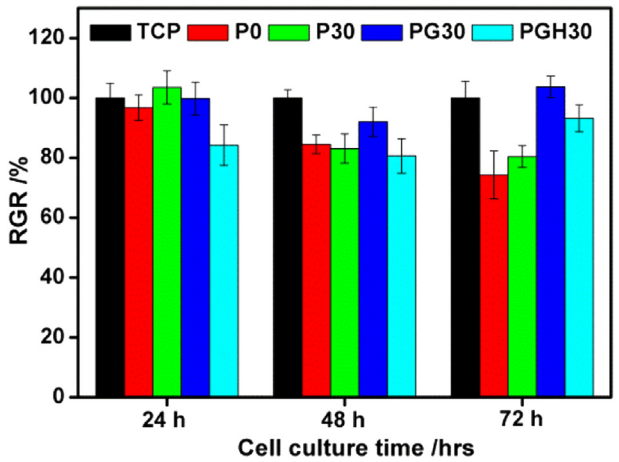

Fig. 6. RGR/% of the L929 cells cultured in the extract substrates of PCL-based electrospun membranes.

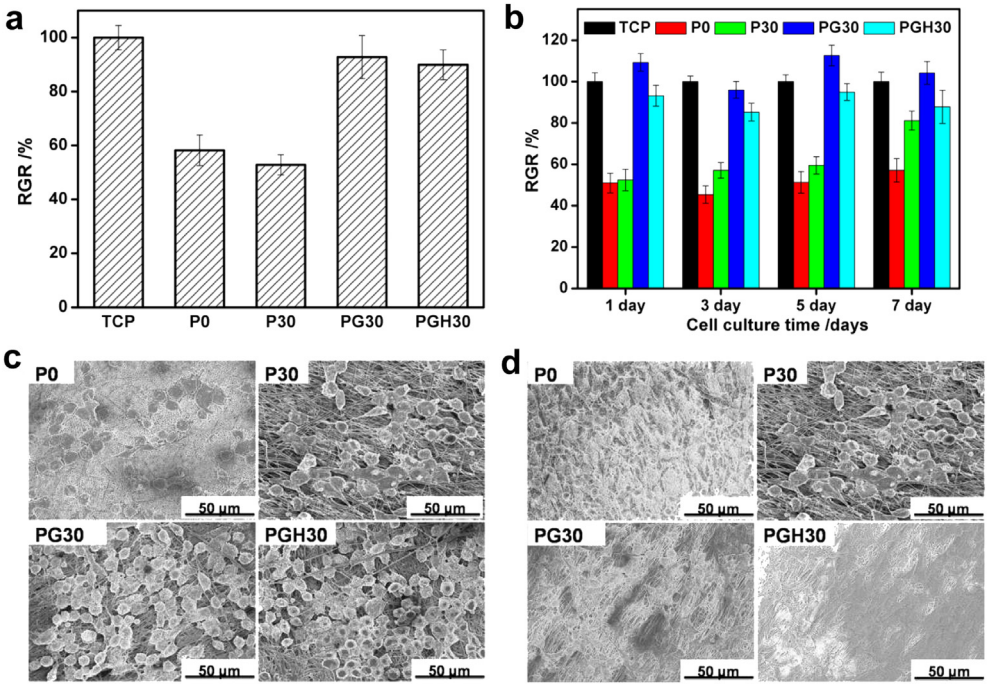

Fig. 7. RGR of L929 cells (a) adhered for 4 h and (b)proliferated for 1, 3, 5, and 7 days on PCL-MNA nanofiber membranes. SEM micrographs of L929 fibroblasts cultured on (c) membranes with different components for 1 day and (d) for 7days.

was sufficient amount of bioactive drug released to substantially inhibit bacterial growth.

3.10. In vivo experiment: tissue compatibility and biodegradation evolution

During the experiment, all the rabbits remained in good health and showed no wound complications. For all the membranes, no acute or chronic inflammation or necrosis and adverse tissue reactions were identified at any time period at the implant sites. Hematoxylin and eosin staining results are shown in Fig. 10. Fig. 11 shows the longitudinal section morphological changes of these membranes at weeks 1, 12, and 24 after implantation. For all the 4 membranes, degradation was faster *in vivo* than *in vitro*.

One week post operation, no neutrophils were observed around the 4 kinds of nanofiber membranes, indicating that no obvious acute inflammation occurred. Some mononuclear phagocytes as well as a small number of capillaries and granulation tissue

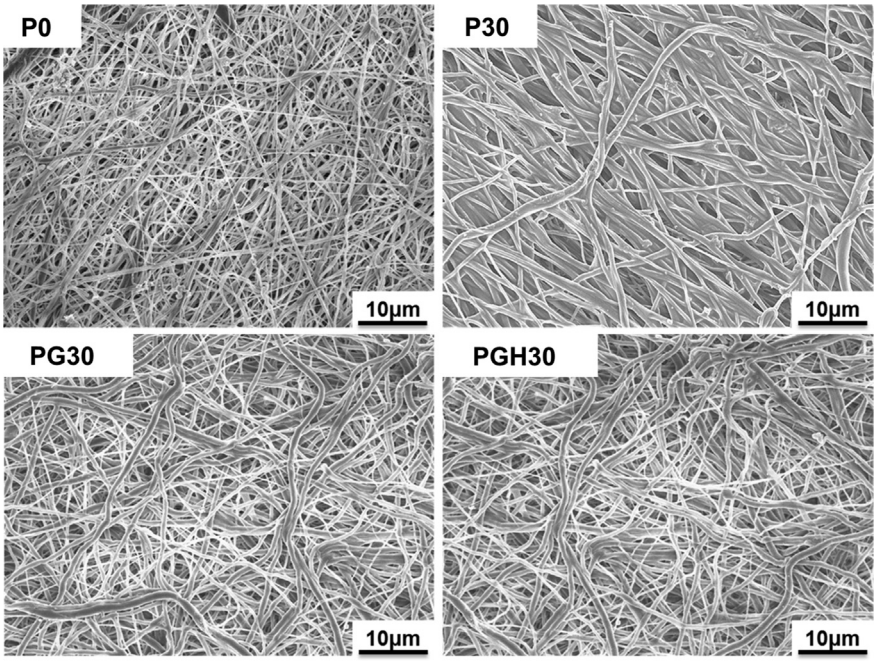

Fig. 8. The SEM micrograph of the opposite side of the cells-seeded membranes after seeding cells on the electrospun PCL-MNA nanofiber membranes for 3 days.

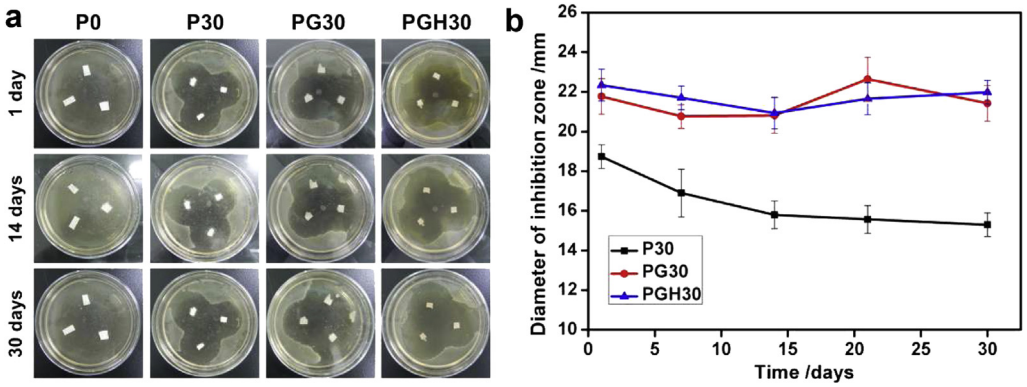

Fig. 9. Inhibition of bacterial growth on agar plates: (a) Inhibition zone surrounding the PCL-based membranes after incubation bacterial for 30 days in anaerobic conditions at 37 °C; (b) The diameter of inhibition zone of the different PCL-based membranes to the bacterial at different incubation time.

gathered around the membranes. Fibroblasts in a particular orientation can be observed in the surrounding tissue, illustrating that the fibrosis/fibrous capsule was forming. The gross view and longitudinal section of the P0 biopsy show an integrated structure after 1 week of embedding. SEM (Fig. 11) showed that the diameter and distribution of the P0 nanofibers had not changed. Compared to P0, the membrane surface began to degrade and the tissue started to migrate inside of P30 (indicated by arrow). There were

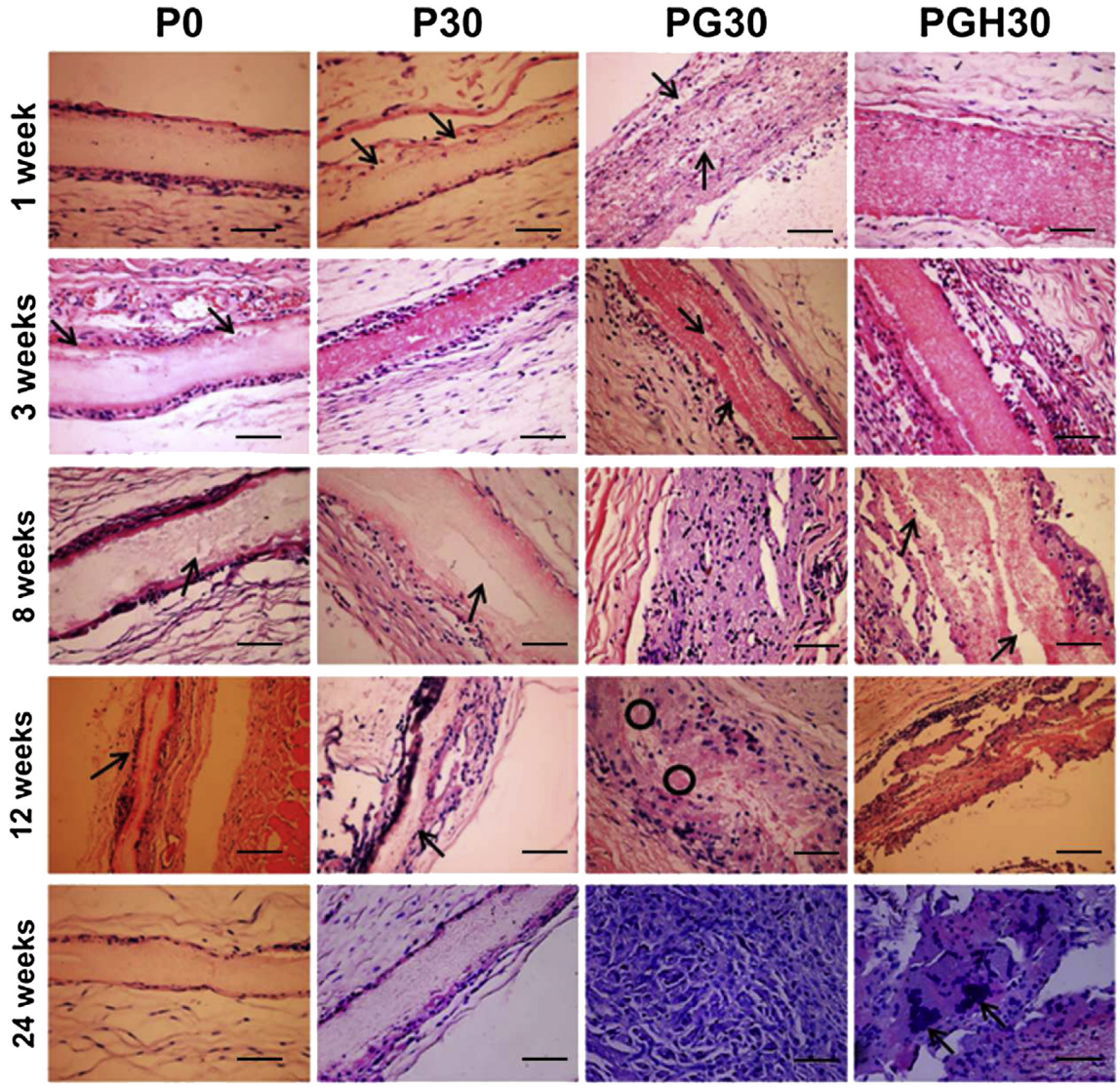

Fig. 10. Histological micrographs of PCL-based nanofiber membranes with H&E staining (length of scale bar = 100 μm).

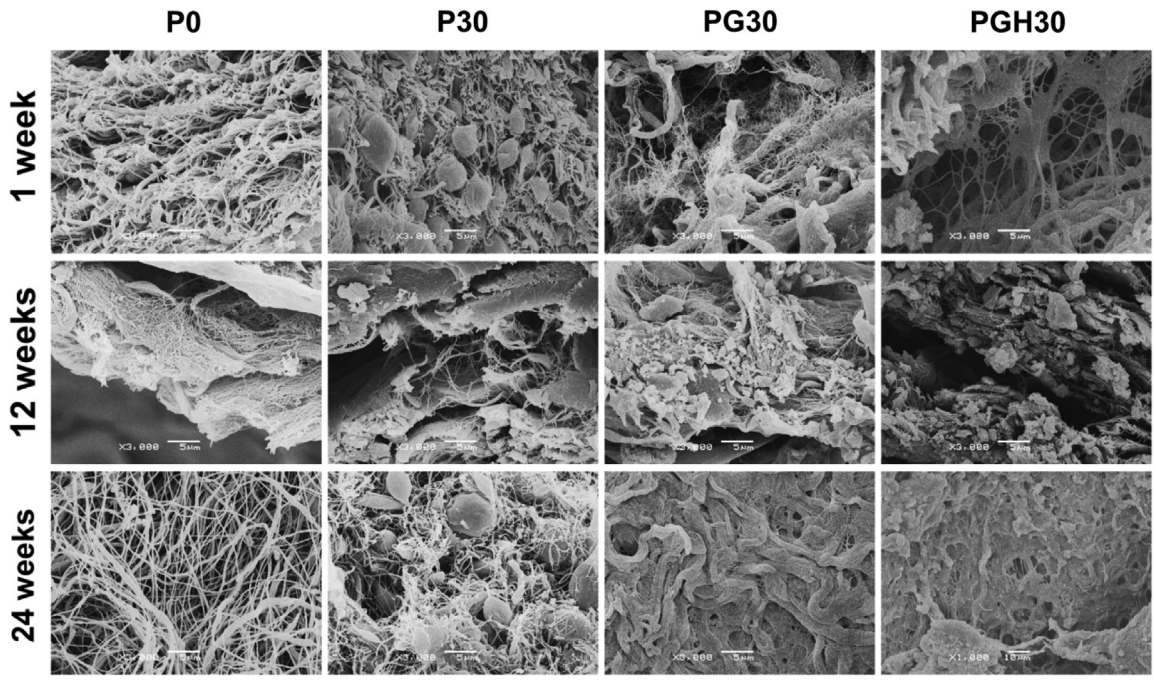

Fig. 11. Morphology of longitudinal section of the PCL-based membranes after subcutaneous implantation: SEM images at 1, 12 and 24 weeks.

more blood capillaries and granulation tissues around P30 than around P0. SEM image showed a large number of red blood cells distributed in the nanofibers. For PG30, the membrane showed a translucent appearance. Degradation occurred not only on surface, but also inside of the membrane as per the histological and SEM observations. Some collagen fibers were intertwined with the nanofibers, and the nanofiber diameter decreased. Because gelatin dissolves very quickly, vascular components quickly grew into the membrane, and some histocytes was transported inside of the membranes as ingrowths of blood vessels, leading to both surface and bulk degradation (indicated by arrow). Tissue section images reflected that the number of tissue cells inside of PGH30 was lower than that in PG30, demonstrating that degradation of PGH30 *in vivo* is slower than that of PG30.

Three weeks after subcutaneous preparation, the number of monocytes around the membrane greatly increased. Granulation tissue, new thin-walled blood vessels, and fibrous capsule developed, accompanied by a small number of macrophages. For P0, the internal migration phenomenon of the fibrous tissue around membrane appeared to be more obvious, and further degradation appeared on the material surface (indicated by arrow) compared with that after 1 week. P30 appeared similar to P0 after 3 weeks. However, PG30 showed obvious and stratified degradation both on the surface and inside of the membrane (indicated by arrow). Compared with PG30, the degradation speed of PGH30 was slightly slower. The hollow and stratified phenomenon was not observed in the middle region of the PGH30, as observed on the image of PG30. Fibroblasts and phagocytes did not penetrate into the membrane, and PG30 and PGH30 retained their barrier function after 3 weeks.

After degradation for 8 weeks, P0 was surrounded by a large number of fibroblasts, monocytes, and multinucleated giant cells, as well as new blood vessels and granulation tissues. Some hollow space inside of the membrane appeared (indicated by arrow), but no cells were inside P0. Membrane thickness and the appearance of P30 were similar to those of P0. The barrier function of P0 and P30 were well-maintained at 8 weeks. Degradation was also observed in the inner part of the P30 membrane (indicated by arrow). However, few microphages were around P30, similarly to P0. P30 induced the formation of a much thinner inflammatory fibrous capsule than P0 did. For PG30, the material was replaced by a fibrous tissue. A mass of fibroblasts, monocytes, and multinucleated giant cells, as well as blood vessels were observed in the inner part of the membrane. Integration of the interface between the membrane and tissue was achieved. The blocking function of PG30 completely disappeared at 8 weeks. Compared to PG30, although a large amount of hollow space appeared inside the membrane, the cells were not present throughout the membrane. Again, the degradation rate of PGH30 was slower than that of PG30.

In tissue section images at 12 weeks, fibrous capsules (indicated by arrow) were observed near the P0 and P30 became thicker, and the membranes were thinner than those at 8 weeks. The vascular tissue around the membranes increased in richness. A very large number of macrophagocytes accumulated and covered the membrane surface. For PG30, only some pieces of the material (indicated by blank circles) were observed. The PGH30 was also degraded into some debris after 12 week.

After 24 weeks, a large number of macrophages gathered (indicated by arrow), and only segments that had been covered by macrophages could be observed. Even 24 weeks after implantation, the integrity of both P0 and P30 was well maintained. Based on the cross-section images of P0 and P30, there was no infiltration of cells inside the membranes until 12 weeks. However, the fibrous tissue had already grown into the PG30 and PGH30 after 12 weeks. Only a small amount of nanofibers distributed in the fibrous tissue could be observed on the SEM image (Fig. 11). The nanofibers nearly completely disappeared. Collagen fibers replaced the membrane materials after 24 weeks, according to the SEM images.

4. Discussion

Four types of electrospinning membranes containing PCL as the main component for GTR application were examined in this study. Incorporation of different components showed that a series of changes in the macroscopic and microscopic structure occurred,

resulting in different physical properties and related biological effects.

4.1. Macro- and micro-structure changes as the result of different components

Generally, when the conductivity of a solution increases, a larger number of electric charges are carried by the electrospinning jet. Thus, higher elongation forces are imposed on the jet under the electrical field. Thus, the jet path becomes longer, and more stretching of the solution is induced [27]. Moreover, bending instability can be increased during electrospinning. Both higher elongation forces and greater bending instability will result in fibers with lower diameter.

PCL, a nonionic synthetic polymer, when dissolved in organic solvent, does not ionize in solution. By adding MNA, the viscosity and surface tension of the PCL solution decreased, while electric conductivity increased. Thus, the mean nanofiber diameter of P30 was lower than that of P0. Generally, smaller fiber diameter facilitates close fiber stacking. Therefore, the average pore size of P30 decreased. For PG30, both gelatin and MNA were mixed with PCL in the spinning solution. Gelatin is a polyelectrolyte polymer with many ionizable groups such as amino and carboxylic groups, which produce ions when dissolved [28]. Thus, the solution containing gelatin will have a higher charge density on the polymer surface, and the nanofiber diameter will be thinner. However, the fiber diameter distribution of PG30 was non-uniform, and could be divided into thick and thin groups, which occurred because of phase separation during electrospinning. PCL/gelatin solution was homogeneous immediately after mixing, but became opaque and gradually separated into different phases after standing. For the equal mass blend (PCL/gelatin w/w 50:50), phase separation occurred as early as during 3–4 h of standing and formed clear sediment at 8–12 h, which was in accordance with the results of previous studies [16]. We used a spinning speed of 1 mL/h and approximately 20 h was required to fabricate a film approximately 250-μm thick. Thus, the composition and structure of PG30 gradually changed during electrospinning, resulting in an uneven distribution of diameter (Fig. 2 PG30), which leads to unstable performance. In industrial settings involving large-scale and prolonged time for nanofiber production, this limitation must be addressed.

To overcome this issue, a very small amount of HAC was applied to demonstrate the miscibility of the gelatin phase and PCL phase. The mainly reason may be that the incorporation of PCL solution to the gelatin solution will change the pH of the original solution with respect to the gelatin's isoelectric point [29]. Gelatin is a typical protein of polyampholyte containing both amino groups and carboxyl groups, and it has the potential capability to respond to the environmental stimulus. As a solvent, HFIP exhibits a stronger acidic character, so gelatin exposes protic groups on the surface and by shields apolar aprotic groups in the interior of the protein in HFIP. However, when the gelatin/HFIP and PCL/HFIP solutions are mixed together, because of exposure to the highly hydrophobic PCL surrounding condition, the gelatin molecules are forced back, exposing their hydrophobic groups so as to interact with the PCL molecules, leading to a slight shift of pH value and zeta potential close to the IP, so the gelatin molecules intent to form compact resembling particles, and may adhere together and form aggregates of increased sizes, which may be large and heavy enough to settle out to the bottom of the bottle from surrounding medium, and resulting in composition and structure of the fibers changed with time. However, by introducing a tiny amount of acid (HAC) to this mixed solution, gelatin is charged positively because of the protonation of amino groups. Gelatin molecules become mutually exclusive, and the stretched gelatin molecular chains could penetrate into the PCL phase and entangle with PCL chains, forming a miscible and transparent solution. Therefore, the most likely molecular level interpretation of the acid-mediated phase stability and solution homogeneity achieved, so compositionally homogeneous hybrid nanofibers was obtained by just adding a tiny amount of HAC to the electrospinning solution (Fig. 2, PGH30). The compositionally homogeneous of the spinning solution is significant for obtaining products with stable performance.

In addition to macro-structure differences, the micro-structure also changed with the introduction of MNA, gelatin, and HAC, including the miscibility between gelatin and PCL, interactions between the polymer matrix and drug molecules, PCL crystallinity, and drug distribution.

The solubility and compatibility of drugs in the drug/polymer/solvent system were determining factors for the electrospun fiber formulation with high drug encapsulation and constant release of the drugs [30]. For P30, PCL macromolecular chains can form different types of HBs with MNA, improving the compatibility and solubility between PCL and MNA. Although PCL is nonpolar and MNA is polar, these substances show good compatibility because of HB interactions. In case of MNA exiting, electrospinning solution conductivity increased, leading to the formation of thinner nanofibers compared to pure PCL nanofibers (P0); thus, PCL crystal formation in P30 was more difficult than that in the PCL nanofibers. Additionally, MNA acted as a plasticizer to restrain PCL crystal stack formation, decreasing PCL crystallization. For the PG30 composite material system, the HB type appears more complicated. Gelatin is composed of 18 types of amino acid proteins. Because there is no regulate repeat segment structure like synthetic polymers, it is hard to use molecular dynamics simulation to predict molecular structure and hydrogen bond types. In addition to HBs between PCL and MNA observed by molecular simulation, HBs between PCL/gelatin and MNA/gelatin also existed. Because the oxygen and nitrogen atom of −OH, −CN, and $-NO_2$ on MNA can HB with the hydrogen atom of −CH, −NH, and −OH on gelatin, and the −NH and −C═O on gelatin can also form HBs with the hydrogen atom of −CH and −OH on MNA, there are more groups that can HB with MNA on gelatin chains than on PCL. Thus, MNA molecules generally aggregate in the gelatin phase. Aggregation induces an increase in MNA crystallinity according to the XRD and DSC results (Fig. 3). Because the electrical conductivity of the gelatin phase is higher than that of PCL, the gelatin phase is generally distributed outside of the nanofiber, and there is more MNA aggregated in the gelatin phase than in the PCL phase; thus, MNA is more likely to migrate to the nanofiber surface during fabrication, and thus more MNA crystal particles are observed on the PG30 surface than on the other samples. In the case of PGH30, the miscibility of PCL and gelatin improved; thus, the MNA distribution in PGH30 was more homogeneous than in PG30, such that there were fewer particles on the PGH30 surface than on PG30 (Fig. 2). Additionally, because of the high miscibility, intramolecular PCL crystallization and MNA aggregation decreased, resulting in lower PCL and MNA crystallization in PGH30 than in PG30.

In conclusion, different composites will result in different interactions among various components, resulting in alternative connections and distributions between the drug and polymer matrix.

4.2. Physical property differences

For membrane application in GTR/GBR therapies, mechanical properties, surface hydrophilicity, and biodegradability are 3 of the most important physical properties. Additionally, drug loading and release properties are very important for inhibiting infection.

For application in tissue regeneration, a porous membrane must provide sufficient mechanical properties such as stress bearing during the surgical procedure (handling and suturing) as well as the ability to withstand *in vivo* stresses and avoid excessive new-tissue deformation. Additionally, the GTR membrane must typically be soaked in saline before the implant surgery to mimic the body-fluid environment, making mechanical properties in the wet state very important. Addition of MNA may increase spinning solution conductivity, decreasing fiber diameter and TS. This can lead to the dense packing of the nanofibers, decreasing the relative displacement between different nanofibers and thus decreasing EB. For PG30 and PGH30, the low mechanical strength of gelatin further reduced the mechanical strength compared to P30. After soaking the membrane in water, some drug was released and the PCL molecule chains were rearranged, resulting in recrystallization and increased TS. This explains why TS in the wet state is slightly higher than that in the dry state.

With respect to the mechanical requirements of GTR membranes, TS values of 0.017 and 2–3 MPa are sufficient [25,26]. TS of PCL-based membranes in our study ranged from 4.1 to 10.0 MPa in the dry state and 3.9–12.6 MPa in the wet state (Table 2). The TS of our PCL-based membranes were sufficient.

The hydrophilicity of biomaterials largely influences cell adhesion and proliferation [31–33]. Because of the hydroxyl on MNA and polar imidazole ring functional groups, as well as amine and carboxylic functional groups on gelatin, incorporation of MNA and gelatin may improve membrane hydrophilicity (see Table 3). The hydrophilicity difference between PG30 and PGH30 were attributed to differences in homogeneity. The incorporation of acetic acid improved nanofiber homogeneity, such that the gelatin content on the top side of PGH30 was lower than that on PG30 fabricated in the gelatin-rich phase, resulting in a higher CA value for PGH30 than for PG30. Additionally, more MNA remained in the center of the PGH30 fiber than in PG30, and therefore, the drug release rate of PGH30 was slower than that of PG30. PGH30 is more suitable for sustained-release of hydrophilic drugs than PG30 is.

In vitro degradation results (see Fig. 5) showed that the hydrophilic drug and gelatin were important for degradation. Because of the very slow degradation rate of PCL within 3 months, the mass loss was mainly attributed to the drug and gelatin. Although the TS of all the membranes decreased slightly, new tissue regeneration can still be supported [26]. In this study, the low degradation rate of PCL, which limits the clinical use of PCL, was significantly increased by the incorporation of the hydrophilic MNA and gelatin.

Drug encapsulation efficiency is highly influenced by the solubility and compatibility of the drug in an electrospun solution. Although MNA is hydrophilic and PCL is hydrophobic, strong HBs can still form on improving their compatibility, according to molecular simulation and FTIR results. Additionally, MNA is highly soluble in the electrospun solution. A relatively high entrapment efficiency of 83.2% was observed for P30. Because the interactions between MNA and gelatin are stronger than those between MNA and PCL, the entrapment efficiency of gelatin-containing samples should be higher than those without gelatin. However, because the drug is more likely to aggregate on the surface of the gelatin-containing samples, the improvement in the entrapment efficiency was limited. The HAC-mediated membrane showed more even drug distribution than the membrane without HAC did, and this improvement is also helpful for improving drug encapsulation efficiency.

It has been demonstrated that both the amount and distribution of amorphous drug and drug particles have a profound influence on the release kinetics [34] Higher amorphous concentrations in the membrane lead to higher release rates and stronger initial bursting, and distributing more drug particles close to or at the membrane surface has the same effect [35].Compared to P30, PG30 preserved higher drug content. Besides, more drugs distributed in the gelatin phase. The degradation rates of gelatin phase is quicker than PCL phase. Both of the high drug content and degradation rates resulted in faster drug release of PG30 than P30. Because of the MNA distribution in PGH30 is more homogeneous than that in PG30, the MNA stayed in the center part of the PGH30 fiber is more than that in PG30, so the drug release rate of PGH30 is slower than that of PG30 (see Fig. 4), so PGH30 is more suitable for sustained release of hydrophilic drugs.

When a material is implanted into a tissue-defect site, infection and inflammation most frequently occurs during the first week. A large initial burst of antibiotic drugs is ideal for eliminating intruding bacteria before they begin to proliferate in the first few days after material implantation. Few microorganisms can survive after an initial burst; however, continued drug release is necessary for preventing the proliferation of their further population and for inhibiting the occurrence of latent infection [36]. The drug release profile of our MNA loading nanofiber membranes adapted to the inflammation cycle characteristics. Additionally, the concentration of the drug released during the first week was sufficiently high to inhibit bacterial growth, but was much lower than the systemic treatment dosage (see ESI S19).

4.3. Biological property changes

In addition to structural and physical properties changes, different material components will also cause biological changes such as those in cellular compatibility, anti-bacterial properties, histocompatibility, and *in vivo* degradability.

Cells in contact with a surface will first attach, adhere, and spread. One side of the GTR/GBR membrane contacts the defect, while the other side contacts the fibrous tissue. Therefore, fibroblast adhesion and proliferation is helpful for wound healing and maintaining the space for defective tissue growth. According to previous studies, hydrophobic surfaces show lower cell adhesion in the initial step of cell culture, and incorporating MNA increased the hydrophilicity of the nanofiber membranes. Cells then proliferated on the rough surface [37]. Drug crystals may be exposed to the fiber surface during degradation, producing a rough nanofiber surface. These factors result in the faster proliferation of L929 on P30 than on P0. Additionally, a large number of hydrophilic groups such as $-NH_3$ and $-COOH$, as well as a number of cell-recognition domains on the gelatin chains, greatly improved cell attachment and proliferation. Although fewer cells proliferated on the surface of PGH30 than on PG30 within 7 days, the small amount of acetic acid slightly influenced the cytotoxicity of the membrane. However, the number of cells on the surface of PGH30 was higher than that in case of P30, and the RGR increased to 93% on the 7th day, demonstrating that PGH30 is still an excellent cell-friendly material (see Fig. 7).

Bacterial inhibition experiments (see Fig. 9) were conducted to examine the effects of matrix components on the antibacterial properties of different PCL-based nanofiber membranes at the same drug-loaded contents. Because gelatin degrades very quickly, drug present in the gelatin phase will quickly diffuse onto the plate; thus, the initial antibacterial ability of PG30 and PGH30 was better than that of P30. Because of the strong interaction between drug and gelatin, most drugs exist in the gelatin phase. Thus, PG30 and PGH30 released more drug than P30 did, resulting in the stronger antibacterial property.

To assess the inflammatory reaction of these nanofiber membranes and determine whether a local high concentration of MNA and HAC contained in PGH30 could mitigate an *in vivo* host response, we performed a subcutaneous implant study (Figs. 10 and 11). MNA addition improved membrane hydrophilicity, increasing

the degradation speed. In addition, MNA may prevent histiocyte and monocyte aggregation, and thus incorporation of MNA may restrain host reaction to some extent.

The degradation rate of membranes directly affected the maintenance of barrier function and tissue regeneration space. As a result of *in vivo* implantation, the typical foreign body response occurred, which involved the accumulation of cells, such as macrophages. Free radicals, acidic products, or enzymes produced by these cells during the foreign body response; these factors may accelerate degradation [38], increasing the *in vivo* degradation rate compared to the *in vitro* rate. With the very fast dissolution of gelatin, a mass of fibroblasts, monocytes, and multinucleated giant cells, as well as blood vessels, can easily grow into the inside of the membrane, resulting in a fast degradation speed for PG30 and PGH30. The HAC-mediated homogeneous composite is also helping for maintaining the membrane barrier function. The GTR membrane should preserve its shield function for 3–6 months to protect hard tissue regeneration. Both P0 and P30 maintained their block function for as long as 24 weeks. The slow degradation rate of P0 and P30 membrane suggested that the requirements of physical integrity during tissue regeneration were satisfied. However, gelatin incorporation dramatically increased degradation. According to our results, although the degradation rate of the HAC-mediated homogeneous membrane was slower than that without the HAC sample, while the gelatin reached 50 wt% of the total weight of gelatin and PCL, the membrane barrier function can only be maintained for 8 weeks. Thus, gelatin content must be reduced for GTR/GBR application.

5. Conclusions

This study comprehensively and systematically investigated the structure and performances of 4 types of PCL-based electrospun nanofiber membranes to select a suitable material system for application in GTR/GBR treatment. The TS of all the membranes satisfied the requirement of the GTR membrane. The PCL-based polymer matrix was suitable for preparing the MNA loading GTR/GBR membrane because the drug encapsulation efficiency was relatively high and the drug release profile was consistent with the inflammation cycle characteristics. Incorporation of gelatin and MNA greatly improved hydrophilicity, leading to improvements in cell biocompatibility. Trace amounts of HAC effectively prevented phase separation in spinning solution, resulting in homogeneous gelatin/PCL nanofibers and uniform drug dispersion. Drug encapsulation efficiency increased and the drug release speed decreased with HAC incorporation. A high local drug concentration and the very small amount of HAC caused no adverse tissue reactions. Thus, the PCL/gelatin/MNA/HAC composite is very suitable for preparing the GTR/GBR membrane. However, the proportion of gelatin should be reduced to maintain membrane integrity within 3 months. Membrane performance should be further confirmed in a periodontal regeneration infection model. Additionally, this drug delivery system may be broadly applicable to any therapeutic approach in which controlled drug delivery is necessary, such as wound healing, prevention of post-surgical adhesions, and tissue engineering applications.

Acknowledgments

This work was supported by the National Natural Science Foundation of China (51303014, 81330043), Beijing Nova Program (Z131102000413015), National Outstanding Youth Science Fund (50725310), The Ministry of Science and Technology of the China (2012BAI10B02), and Beijing Municipal Training Programme Foundation for the Talents (2013D00303400041).

Appendix A. Supplementary data

Supplementary data related to this article can be found online at http://dx.doi.org/10.1016/j.polymdegradstab.2014.07.017.

References

[1] Kuo SM, Chang SJ, Chen TW, Kuan TC. Guided tissue regeneration for using a chitosan membrane: an experimental study in rats. J Biomed Mater Res Part A 2006;76A:408–15.
[2] Bottino MC, Thomas V, Schmidt G, Vohra YK, Chu TMG, Kowolik MJ, et al. Recent advances in the development of GTR/GBR membranes for periodontal regeneration—a materials perspective. Dent Mater 2012;28:703–21.
[3] Sill TJ, Von RHA. Electrospinning: applications in drug delivery and tissue engineering. Biomaterials 2008;29:1989–2006.
[4] Stamatialis DF, Papenburg BJ, Gironés M, Saiful S, Bettahalli SN, Schmitmeier S, et al. Medical applications of membranes: drug delivery, artificial organs and tissue engineering. J Membr Sci 2008;308:1–34.
[5] Gentile P, Chiono V, Tonda-Turo C, Ferreira AM, Ciardelli G. Polymeric membranes for guided bone regeneration. Biotechnol J 2011;6:1187–97.
[6] Bergsma J, Bruijn WD, Rozema F, Bos R, Boering G. Late degradation tissue response to poly(L-lactide) bone plates and screws. Biomaterials 1995;16:25–31.
[7] Fujihara K, Kotaki M, Ramakrishna S. Guided bone regeneration membrane made of polycaprolactone/calcium carbonate composite nano-fibers. Biomaterials 2005;26:4139–47.
[8] Yang F, Both SK, Yang X, Walboomers XF, Jansen JA. Development of an electrospun nano-apatite/PCL composite membrane for GTR/GBR application. Acta Biomater 2009;5:3295–304.
[9] Chen L. The study of biodegradation of PCL&ITS scaffold fabrication methods; 2007. The Master Degree Dissertation of Dong Hua University.
[10] Gunn J, Zhang M. Polyblend nanofibers for biomedical applications: perspectives and challenges. Trends Biotechnol 2010;28:189–97.
[11] Lee J, Tae G, Kim YH, Park IS, Kim SH. The effect of gelatin incorporation into electrospun poly(L-lactide-co-epsilon-caprolactone) fibers on mechanical properties and cytocompatibility. Biomaterials 2008;29:1872–9.
[12] Gautam S, Dinda AK, Mishra NC. Fabrication and characterization of PCL/gelatin composite nanofibrous scaffold for tissue engineering applications by electrospinning method. Mater Sci Eng C 2013;33:1228–35.
[13] Powell HM, Boyce ST. Engineered human skin fabricated using electrospun collagen-PCL blends: morphogenesis and mechanical properties. Tissue Eng Part A 2009;15:2177–87.
[14] Zhang YZ, Feng Y, Huang ZM, Ramakrishna S, Lim CT. Fabrication of porous electrospun nanofibres. Nanotechnology 2006;17:901–8.
[15] Kwon IK, Matsuda T. Co-electrospun nanofiber fabrics of poly(L-lactide-co-ε-caprolactone) with type I collagen or heparin. Biomacromolecules 2005;6:2096–105.
[16] Feng B, Tu HB, Yuan HH, Peng HG, Zhang YZ. Acetic-Acid-Mediated miscibility toward electrospinning homogeneous composite nanofibers of GT/PCL. Biomacromolecules 2012;13:3917–25.
[17] Coello R, Charlett A, Wilson J, Ward V, Pearson A, Borriello P. Adverse impact of surgical site infections in English hospitals. J Hosp Infect 2005;60:93–103.
[18] Zamani M, Morshed M, Varshosaz J, Jannesari M. Controlled release of metronidazole benzoate from poly ε-caprolactone electrospun nanofibers for periodontal diseases. Eur J Pharm Biopharm 2010;75:179–85.
[19] Yu DG, Chian W, Wang X, Li XY, Li Y, Liao YZ. Linear drug release membrane prepared by a modified coaxial electrospinning process. J Membr Sci 2013;428:150–6.
[20] Reise M, Wyrwab R, Müllerb U, Zylinski M, Völpel A, Schnabelrauch M, et al. Release of metronidazole from electrospun poly(l-lactide-co-d/l-lactide) fibers for local periodontitis treatment. Dent Mater 2012;28:179–88.
[21] Kurtis B, Ünsal B, Çetiner D, Gültekin E, Özcan G, Çelebi N, et al. Effect of polylactide/glycolide (PLGA) membranes loaded with metronidazole on periodontal regeneration following guided tissue regeneration in dogs. J Periodontol 2002;73:694–700.
[22] Chong EJ, Phan TT, Lim IJ, Zhang YZ, Bay BH, Ramakrishna S, et al. Evaluation of electrospun PCL/gelatin nanofibrous scaffold for wound healing and layered dermal reconstitution. Acta Biomater 2007;3:321–31.
[23] Wang R, Ma J, Zhou X, Wang Z, Kang H, Zhang L, et al. Design and preparation of a novel cross-linkable, high molecular weight, and bio-based elastomer by emulsion polymerization. Macromolecules 2012;45:6830–9.
[24] Thakur R, Florek C, Kohn J, Michniak B. Electrospun nanofibrous polymeric scaffold with targeted drug release profiles for potential application as wound dressing. Int J Pharm 2008;364:87–93.
[25] Ueyama Y, Ishikawa K, Mano T, Koyama T, Nagatsuka H, Suzuki K, et al. Usefulness as guided bone regeneration membrane of the alginate membrane. Biomaterials 2002;23:2027–33.
[26] Li JD, Zuo Y, Cheng XM, Yang WH, Wang HN, Li YB. Preparation and characterization of nano-hydroxyapatite/polyamide 66 composite GBR membrane with asymmetric porous structure. J Mater Sci Mater Med 2009;20:103.
[27] Ramakrishna S, Fujihara K, Teo WE, Lim TC, Ma Z. An introduction to electrospinning and nanofibers. Singapore: World Scientific; 2005.

[28] Zhang Y, Ouyang H, Lim CT, Ramakrishna S, Huang ZM. Electrospinning of gelatin fibers and gelatin/PCL composite fibrous scaffolds. Biomed Mater Res Part B Appl Biomater 2005;72:156–65.
[29] Mohanty B, Bohidar HB. Systematic of alcohol-induced simple coacervation in aqueous gelatin solutions. Biomacromolecules 2003;4:1080–6.
[30] Zeng J, Yang LX, Liang QZ, Zhang XF, Guan HL, Xu XL, et al. Influence of the drug compatibility with polymer solution on the release kinetics of electrospun fiber formulation. J Control Release 2005;105:43–51.
[31] Fang ZD, Fu WG, Dong ZH, Zhang XM, Gao B, Guo DQ, et al. Preparation and biocompatibility of electrospun poly(l-lactide-co-ε-caprolactone)/fibrinogen blended nanofibrous scaffolds. Appl Surf Sci 2011;257:4133–8.
[32] Wu L, Li H, Li S, Li XR, Yuan XY, Li XL, et al. Composite fibrous membranes of PLGA and chitosan prepared by coelectrospinning and coaxial electrospinning. Biomed Mater Res A 2010;92:563–74.
[33] Zhou S, Peng H, Yu X, Zheng X, Cui W, Zhang Z, et al. Preparation and characterization of a novel electrospun spider silk fibroin/poly(d, l-lactide) composite fiber. Phys Chem B 2008;112:11209–16.
[34] Xiang A, McHugh AJ. A generalized diffusion–dissolution model for drug release from rigid polymer membrane matrices. J Membr Sci 2010;366:104–15.
[35] Xiang A, McHugh AJ. Quantifying sustained release kinetics from a polymer matrix including burst effects. J Membr Sci J 2011;371:211–8.
[36] Kim K, Luu YK, Chang C, Fang DF, Hsiao BS, Chu B, et al. Incorporation and controlled release of a hydrophilic antibiotic using poly (lactide-co-glycolide)-based electrospun nanofibrous scaffolds. J Control Release 2004;98:47–56.
[37] Anselme K. Osteoblast adhesion on biomaterials. Biomaterials 2000;21:667–81.
[38] Tracy M, Ward K, Firouzabadian L, Wang Y, Dong N, Qian R, et al. Factors affecting the degradation rate of poly(lactide-co-glycolide) microspheres in vivo and in vitro. Biomaterials 1999;20:1057–62.